Laminar organization of neocortical activities during systemic anoxia

Antoine Carton-Leclercq, Sofia Carrion-Falgarona, Paul Baudin, Pierre Lemaire, Sarah Lecas, Thomas Topilko, Stéphane Charpier, Séverine Mahon

▶ **To cite this version:**

Antoine Carton-Leclercq, Sofia Carrion-Falgarona, Paul Baudin, Pierre Lemaire, Sarah Lecas, et al.. Laminar organization of neocortical activities during systemic anoxia. Neurobiology of Disease, 2023, 10.1016/j.nbd.2023.106345 . hal-04642062

HAL Id: hal-04642062

https://hal.sorbonne-universite.fr/hal-04642062v1

Submitted on 9 Jul 2024

HAL is a multi-disciplinary open access archive for the deposit and dissemination of scientific research documents, whether they are published or not. The documents may come from teaching and research institutions in France or abroad, or from public or private research centers.

L'archive ouverte pluridisciplinaire **HAL**, est destinée au dépôt et à la diffusion de documents scientifiques de niveau recherche, publiés ou non, émanant des établissements d'enseignement et de recherche français ou étrangers, des laboratoires publics ou privés.

Distributed under a Creative Commons Attribution - NonCommercial - NoDerivatives 4.0 International License

Neurobiology of Disease 188 (2023) 106345

Contents lists available at ScienceDirect

Neurobiology of Disease

journal homepage: www.elsevier.com/locate/ynbdi

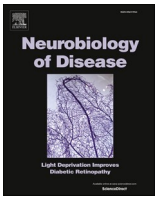

Laminar organization of neocortical activities during systemic anoxia

Antoine Carton-Leclercq, Sofia Carrion-Falgarona, Paul Baudin, Pierre Lemaire, Sarah Lecas, Thomas Topilko, Stéphane Charpier [1], Séverine Mahon [*,1]

Sorbonne Université, Paris Brain Institute - Institut du Cerveau, ICM, INSERM, CNRS, APHP, Pitié-Salpêtrière Hospital, Paris, France

ARTICLE INFO

Keywords:
Anoxia
Neocortex
Excitability
Anoxic depolarization
Pyramidal neurons

ABSTRACT

The neocortex is highly susceptible to metabolic dysfunction. When exposed to global ischemia or anoxia, it suffers a slowly propagating wave of collective neuronal depolarization that ultimately impairs its structure and function. While the molecular signature of anoxic depolarization (AD) is well documented, little is known about the brain states that precede and follow AD onset. Here, by means of multisite extracellular local field potentials and intracellular recordings from identified pyramidal cells, we investigated the laminar expression of cortical activities induced by transient anoxia in rat primary somatosensory cortex. Soon after the interruption of brain oxygenation, we observed a well-organized sequence of stereotyped activity patterns across all cortical layers. This sequence included an initial period of beta-gamma activity, rapidly replaced by delta-theta oscillations followed by a decline in all spontaneous activites, marking the entry into a sustained period of electrical silence. Intracellular recordings revealed that cortical pyramidal neurons were depolarized and highly active during high-frequency activity, became inactive and devoid of synaptic potentials during the isoelectric state, and showed subthreshold composite synaptic depolarizations during the low-frequency period. Contrasting with the strong temporal coherence of pre-AD activities along the vertical axis of the cortical column, the onset of AD was not uniform across layers. AD initially occurred in layer 5 or 6 and then propagated bidirectionally in the upward and downward direction. Conversely, the post-anoxic waves that indicated the repolarization of cortical neurons upon brain reoxygenation did not exhibit a specific spatio-temporal profile. Pyramidal neurons from AD initiation site had a more depolarized resting potential and higher spontaneous firing rate compared to superficial cortical cells. We also found that the propagation pattern of AD was reliably reproduced by focal injection of an inhibitor of sodium-potassium ATPases, suggesting that cortical AD dynamics could reflect layer-dependent variations in cellular metabolic regulations.

1. Introduction

Close regulation of cellular energy metabolism is crucial for the normal functioning of the brain, which despite its small relative size is one of the most metabolically costly organs, accounting for 20–25% of the basal oxygen consumption in adult humans (Clarke and Sokoloff, 1999). About 80% of brain energy is consumed for the maintenance of synaptic transmission, restoration of transmembrane electrochemical gradients, modulation of neuronal excitability and intracellular signaling (Attwell and Laughlin, 2001; Hofmeijer and van Putten, 2012; Watts et al., 2018). During ischemia or anoxia, the severe disruption of oxygen supply to the brain leads to the rapid depletion of ATP reserves and impairs the activity of sodium-potassium ATPases (Na^+-K^+ ATPases) responsible for maintaining ion homeostasis (Lipton, 1999; Somjen, 2001). This results in a significant redistribution of ions across the neuronal membrane, involving large influxes of Na^+ and calcium (Ca^{2+}) into neurons, as well as a massive efflux of K^+. The accumulation of K^+ in the interstitial medium, coupled with an excessive release of glutamate, causes anoxic depolarization (AD), a near-complete depolarization of neurons that slowly propagates in the metabolically compromised tissue initiating cell death processes (Nedergaard and Hansen, 1993; Martin et al., 1994; Somjen, 2001; Dreier, 2011;

Abbreviations: AD, Anoxic Depolarization; AP, Action Potential; $Ca2^+$, calcium; DC, Direct Current; ECoG, electrocorticogram; $EtCO_2$, End-tidal Carbon Dioxide Concentration; K^+, potassium; LFP, Local Field Potential; Na^+, sodium; pAR, post-Anoxic Repolarization; Rin, membrane input resistance; S1, primary somatosensory cortex; SpO_2, arterial oxygen saturation; Vm, membrane potential; WAD, ECoG Wave of Anoxic Depolarization; WpAR, ECoG Wave of post-Anoxic Repolarization.

* Corresponding author.
E-mail address: severine.mahon@upmc.fr (S. Mahon).

[1] These authors contributed equally to this work.

https://doi.org/10.1016/j.nbd.2023.106345
Received 11 July 2023; Received in revised form 1 November 2023; Accepted 1 November 2023
Available online 3 November 2023
0969-9961/© 2023 The Authors. Published by Elsevier Inc. This is an open access article under the CC BY-NC-ND license (http://creativecommons.org/licenses/by-nc-nd/4.0/).

Pietrobon and Moskowitz, 2014). However, this process can be reversed since rapid reoxygenation or reperfusion of the brain can reactivate Na^+-K^+ pumps, repolarize neurons and restore synaptic transmission, as was recently observed in a rodent model of transient asphyxia (Schramm et al., 2020; Charpier, 2023).

The damaging effects associated with the propagation of AD do not occur immediately after the beginning of anoxia (Pietrobon and Moskowitz, 2014; Charpier, 2023). Accumulating evidence from clinical studies on patients experiencing global cerebral ischemia after the cessation of life-sustaining treatments, and from investigations in animal models, indicates that electroencephalographic (EEG) activity undergoes a series of transformations before the onset of AD. These transformations include a brief period of high-frequency oscillations, followed by a slowing down and attenuation of cortical activities before the entry into a state of complete inactivity (isoelectric state) (Borjigin et al., 2013; Schramm et al., 2020; Xu et al., 2023; for reviews, Charpier, 2023; Shlobin et al., 2023). The different patterns of spontaneous activity observed during this process, particularly the initial surge of high-frequency oscillations resembling activity associated with conscious waking, have been suggested to reflect varying levels of cortical processing at near-death (Xu et al., 2023). However, how these peri-mortem activities get organized within the neocortex and their corresponding neuronal correlates remain unknown.

The sensitivity to anoxia varies across cell types and brain structures (Lipton, 1999; Andrew et al., 2017). In this regard, recent optical imaging experiments conducted on anesthetized mice breathing nitrogen showed that AD was preferentially triggered in the somatosensory cortex rather than in thalamus or midbrain, highlighting the high vulnerability of the neocortex to anoxia (Bogdanov et al., 2016). However, the initiation site and propagation profile of the anoxic process across cortical layers are still debated. While previous *in vitro* studies have suggested that ADs induced by oxygen-glucose deprivation or brief exposure to Na^+-K^+ ATPase antagonist primarily originated in superficial layers (Basarsky et al., 1998; Jarvis et al., 2001; Joshi and Andrew, 2001), a recent study on somatosensory cortex slices, showing a preferential emergence of AD from layer 4 (L4) under ischemia-like conditions, did not confirm this finding (Juzekaeva et al., 2017). Similarly, an *in vivo* investigation, employing pharmacological stimuli to increase extracellular K^+ concentration, reported a different site of initiation located in deep cortical layers (Richter and Lehmenkühler, 1993). These seemingly contradictory findings could be attributed to variations in experimental conditions and the variety of stimuli used to trigger AD.

Here, we revisited this issue by investigating *in vivo* the organization and dynamics of cortical activities within the different layers of the primary somatosensory cortex in rats undergoing a systemic and reversible anoxia. We found that the successive cortical states that preceded AD were remarkably similar across layers. In contrast, AD showed a preferential site of initiation in L5, or to a lesser extent in L6, from which it propagated bidirectionally to the brain surface and white matter. This propagation pattern was closely reproduced by local injection of a Na^+-K^+ ATPase antagonist, suggesting a key role for the early loss of transmembrane electrochemical gradients in the onset and propagation of the anoxic process.

2. Materials and methods

Experiments received approval (APAFIS no. 18003–2019051019017280) from the French Ministry for Research and the *Charles Darwin* Ethics Committee (C2EA-05) and were carried out in accordance with the guidelines of the European Union (directive 2010/63/EU). Every precaution was taken to minimize stress and the number of animals used in each series of experiments. All experimental procedures complied with ARRIVE guidelines on animal research.

2.1. Animal preparation and surgery

Experiments were conducted *in vivo* on adult (2–3 months old) Sprague Dawley rats ($n = 42$) of either sex (20 females and 22 males). Animals were first anesthetized by inhalation of isoflurane (3.5%) and underwent tracheotomy for artificial ventilation (room air, 80 breaths/min, 2.6–3.3 ml/cycle) under neuromuscular blockade (gallamine triethiodide, 40 mg/2 h, i.m.). Small craniotomies were made above the left forelimb region of the primary somatosensory cortex (S1) (0.25–2.1 mm posterior to bregma and 2.8–4.0 mm lateral to the midline) (Paxinos and Watson, 2007). Incisions and pressure points were repeatedly (every 2 h) infiltrated with the local anesthetic agent lidocaine (2%; Centravet). After completion of surgery, isoflurane was discontinued but sedation and analgesia were maintained by repeated injection of sufentanil (3 μg/kg every 30 min, i.p.). This anesthetic condition is known to induce a globally stable background activity characterized by low amplitude cortical patterns resembling those encountered during waking (Mahon et al., 2001; Bruno and Sakmann, 2006; Altwegg-Boussac et al., 2017). Heart rate, electrocorticographic activity (ECoG) and local field potentials (LFPs) were continuously recorded to assess the depth of sedation. Oxygen saturation (SpO_2), core temperature (maintained at 37 °C by a feedback-controlled heating blanket) and end-tidal CO_2 ($EtCO_2$) were also monitored throughout the recording sessions (Fig. 1A) with a veterinary vital signs monitor (LifeWindow unit, Digicare). At the end of recordings, animals were euthanized with an overdose of euthasol (40%, i.p.) and perfused for subsequent histological processing.

2.2. Electrophysiology

ECoG activity was captured using a low impedance (~60 kΩ) silver electrode apposed on the dura above S1 and a reference electrode placed on the temporal muscle at the opposite side of the head ($n = 10$ experiments). Signals were amplified with a differential *AC* amplifier (Model 1700; A-M Systems), bandpass filtered between 0.1 Hz and 1 kHz, and digitized at 3 kHz for off-line analysis (CED 1401plus, Cambridge Electronic Design).

Multisite LFPs in S1 were recorded with linear 16-channel (250 μm electrode separation distance, 35 μm site IrOx, 0.2 MΩ; $n = 10$ experiments) or 32-channel (100 μm electrode separation distance, 35 μm site IrOx, 0.7 MΩ; $n = 6$ experiments) silicon probes (ATLAS Neuroengineering®). Silicon probes were inserted perpendicular to the tangent of the S1 surface and penetration into the brain tissue was used as the zero reference to determine the depth of recording sites. LFP signals were amplified using a DigitalLynx amplifier (NeuraLynx®), filtered between 0.1 Hz and 6 kHz, and digitized at 32 kHz.

In separate experiments, paired intracortical direct current (*DC*) recordings ($n = 12$ experiments) were obtained using glass micropipettes, filled with 0.5 M NaCl (10–20 MΩ), inserted in S1 L2–3 (250–400 μm below cortical surface) and L5 (900–1300 μm below cortical surface), with a lateral distance of 300 μm between electrodes. The captured signals were amplified with an Axoclamp 900A amplifier (Molecular Devices), bandpass filtered between *DC* and 3 kHz, and digitized at 10 kHz.

Intracellular recordings ($n = 18$ neurons) from S1 were performed with glass micropipettes filled with 2 M potassium acetate (50–90 MΩ), either in L2–3 (250–500 μm below the cortical surface) or L5 (900–1300 μm below cortical surface). In some experiments ($n = 6$), cortical neurons were labelled by adding 1.5% neurobiotin to the pipette solution (see Supplementary Methods). Current-clamp recordings were amplified with an Axoclamp 900A amplifier (Molecular Devices) operating in bridge mode, bandpass filtered between *DC* and 3 kHz, and digitized at 10 kHz. Recorded neurons were identified as pyramidal cells on the basis of their characteristic firing pattern (regular spiking or intrinsic bursting discharge) in response to suprathreshold steady-state current stimulations (Steriade, 2004) and by their morphological features.

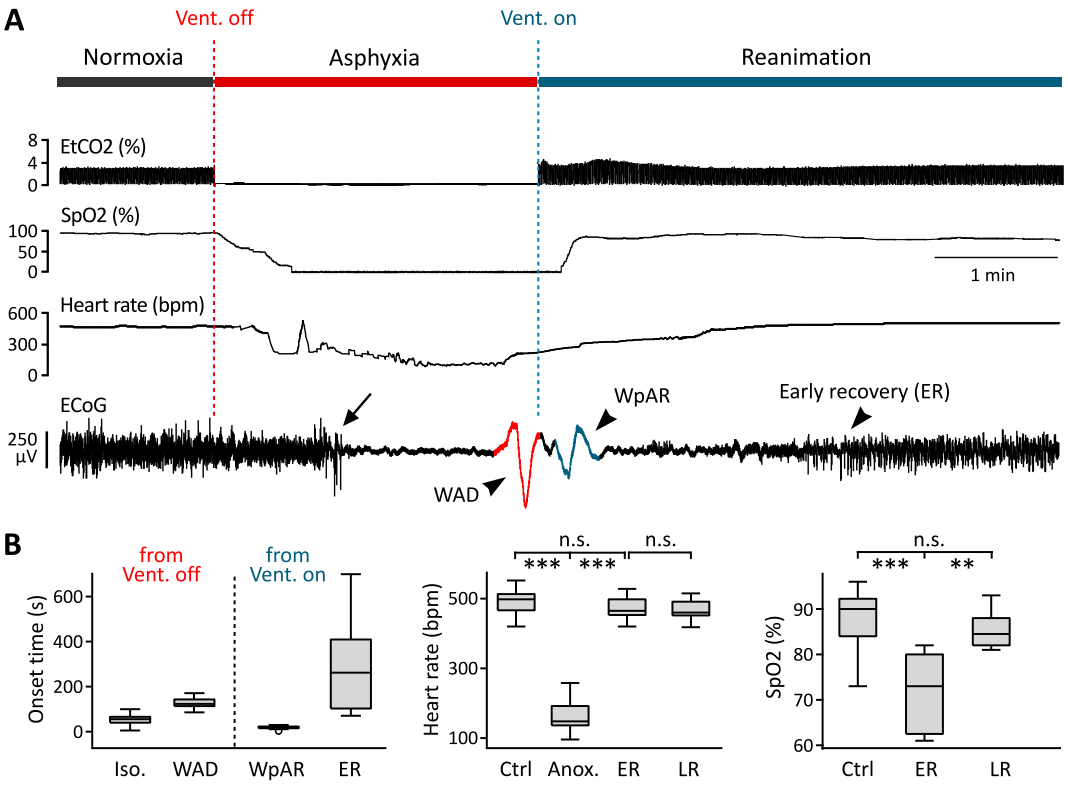

Fig. 1. ECoG dynamics and physiological parameters during the asphyxia and rescue protocols. (A) Typical ECoG record from S1, together with the monitoring of arterial oxygen saturation (SpO_2), end-tidal carbon dioxide concentration ($EtCO_2$) and heart rate, during a control period (Normoxia), the period of oxygen deprivation (Asphyxia) starting with the interruption of mechanical ventilation (Vent. off), and during the rescue process (Reanimation) initiated by the restoration of oxygenation (Vent. on). After a brief episode of slow activities (arrow), the ECoG signal rapidly declined to an isoelectric line before the emergence of a Wave of Anoxic Depolarization (WAD, in red). Restoration of artificial ventilation caused the subsequent appearance of a Wave of post-Anoxic Repolarization (WpAR, in blue), which preceded the gradual return of cortical activity. Early recovery indicates regaining of 90% of the control ECoG amplitude. (B) Specific timings of relevant ECoG states or events (Iso.: isoelectric state) (left), and average values of heart rate (middle) and SpO_2 (right) at the indicated periods (Control, Ctrl; Anox., Anoxia; Early recovery, ER; Late recovery, LR corresponding to 1 h after Vent. on). ** $P < 0.01$, *** $P < 0.001$ (Wilcoxon signed-rank test). Here and in the following figures, upper and lower edges of boxes in boxplots represent 75th and 25th percentiles respectively, middle lines represent the median value and whiskers represent the extreme values. (For interpretation of the references to color in this figure legend, the reader is referred to the web version of this article.)

2.3. Anoxia and rescue protocols

Physiological parameters and multiscale electrophysiological activities were continuously recorded during control periods (normoxia), systemic anoxia and after restoration of oxygen supply (Fig. 1A). Anoxia, induced by a sudden interruption of artificial ventilation in curarized animals (Vent. off), resulted in an instantaneous collapse of $EtCO_2$, followed by a progressive drop in SpO_2, which rapidly (< 1 min) reached undetectable values (< 10 mmHg oxygen pressure, which corresponds to the sensitivity threshold of the LifeWindow monitor) (Fig. 1A). Rescue procedures (reanimation) consisted in restoring the ventilation (Vent. on) just after (4–13 s) the occurrence of an ECoG/LFP wave of anoxic depolarization (WAD/AD), indicative of a collective depolarization of cortical neurons (Schramm et al., 2020; Charpier, 2023). In most protocols ($n = 46$ out of 49), reoxygenation led to the appearance of an ECoG/LFP wave of post-anoxic repolarization (WpAR/pAR), which systematically heralded the restoration of resting membrane potential (Vm) in cortical neurons, as well as synaptic and firing activities in cortical networks (Schramm et al., 2020). In the remaining experiments ($n = 3$), the reanimation process was unable to restore brain activities, leading to cardiac arrest in a few minutes. Some of the animals used in the multisite LFP experiments ($n = 11$) were subjected to two anoxia protocols separated from each other by a period ≥80 min, ensuring recovery of vital signs and a pattern of cortical activity similar in frequency and amplitude to that recorded in normoxic condition. The duration of anoxia was kept similar between the two sessions (see Supplementary Fig. 3B). In paired *DC* recordings experiments, three successive anoxia protocols were performed on each animal ($n = 12$ protocols from 4 rats).

2.4. Analysis of LFP signals

Analysis of LFPs was performed with a combination of Fieldtrip (release 20.200.919) (Oostenveld et al., 2011) and custom-developed scripts in MATLAB (The Mathworks Inc.). To assess the temporal evolution of different relevant frequency bands (delta, 0.5–5 Hz, theta-alpha: 6–10 Hz, and beta-gamma: 15–40 Hz), the frequency content of LFP signals was computed using a multitaper decomposition analysis with a sliding time window of 1 s (Oostenveld et al., 2011; Baudin et al., 2022). Power values within each frequency band were averaged and normalized to their normoxic values, defined as the 5-min period preceding Vent. off (Fig. 2 and Supplementary Fig. 1). The onset time of the maximum power value for a given frequency band was calculated for each recording channel and then averaged along the S1 column. The maximum power values were detected using the MATLAB *findpeaks* function (Supplementary Fig. 1). The beginning of the isoelectric state was determined as the time at which the amplitude of LFP signals reached <10% of their pre-anoxia peak-to-peak values for at least 20 s.

The amplitude of LFP ADs and ouabain-induced depolarizations (ODs, see below) was calculated as the difference between the peak of the initial negative component and the baseline voltage computed over a 5-s period preceding the wave (Fig. 3B). LFP shifts whose amplitude was <5 times the standard deviation (SD) of the normoxic signal were discarded. AD half-width duration and slope (maximum value of the

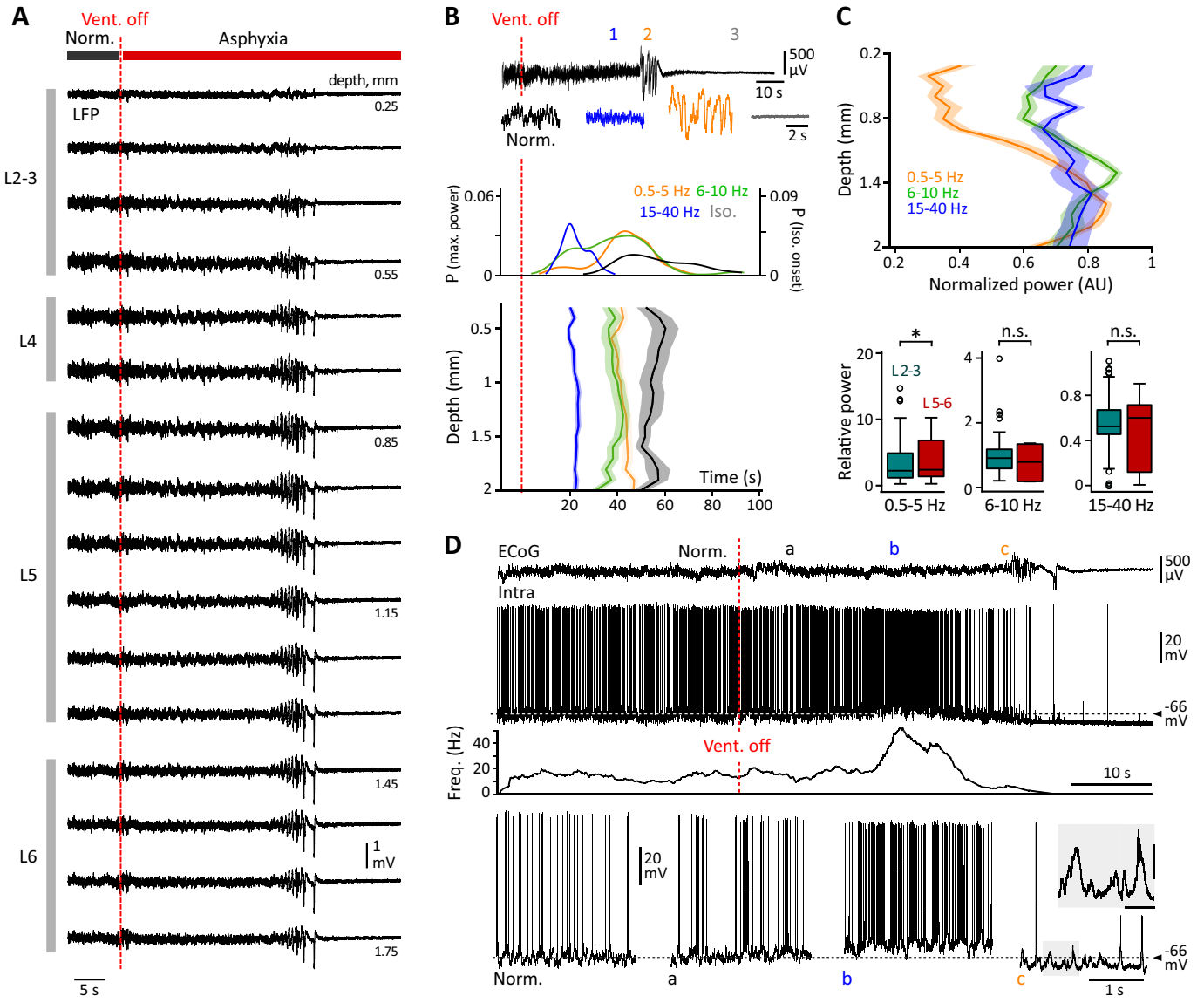

Fig. 2. Anoxia-induced changes in S1 spontaneous activity across layers. (A) LFP activities recorded at different depths of a cortical S1 column with a 32-channel silicone probe (100 µm vertical separation distance between two electrodes), before (Normoxia, Norm.) and after asphyxia induction (Vent. off). Cortical layers (L) are indicated at left. Here, and in the following figures, the recording depth is indicated below the corresponding LFP channel. (B) Representative LFP recording in L5 (top) temporally aligned with the probability densities (P) of maximum power timings for the color-coded frequency bands and of the isoelectric state onset times (grey line) (middle graph). The bottom graph shows, for each frequency band, the mean (± SEM) latency of the maximum powers as a function of cortical depth (n = 27 protocols). The short recordings in color correspond to expanded views of the normoxic period (Norm.) and of the epochs indicated by numbers above the continuous record. The dashed vertical red line indicates Vent. off. (C) Average (± SEM) distribution of maximal power (normalized to their values during the anoxic period) for each frequency band, as a function of cortical depth. The boxplots compare the power of the different frequency bands in L2–3 and L5–6, relative to their corresponding baseline values. (D) Intracellular activity changes over the anoxic period. Top traces: simultaneous recordings of S1 ECoG and intracellular activity of a L5 pyramidal neuron (Intra), before and after Vent. Off. The horizontal dashed line indicates the mean control Vm (−66 mV). The graph below shows the corresponding instantaneous firing rate as a function of time. Lower traces are expanded views of intracellular activity recorded during the periods indicated by letters above the ECoG. Norm. corresponds to the normoxic period before Vent. Off and a, b, c corresponds to the early anoxic, high-frequency and low-frequency periods, respectively. In c, spikes are truncated and the inset is a zoom in the slow Vm fluctuations. Calibrations: 6 mV, 200 ms. ns: non-significant; *: $P < 0.05$. (For interpretation of the references to color in this figure legend, the reader is referred to the web version of this article.)

signal's first derivative after smoothing with a 1 s time window) were measured on the first negative deflection (Fig. 3B). AD and OD onset latencies were respectively calculated as the time difference between their peak negativity and Vent. off, or the onset of ouabain injection. Latency of post-anoxic waves was the time difference between their first positive peak potential and Vent. on. Upward and downward AD (or OD) propagation velocity were calculated as the *ratio* of the distance between electrodes displaying the earliest and latest waves and their time difference.

2.5. Analysis of intracellular and extracellular DC records

Intracellular and extracellular *DC* signals were analyzed with Spike2 software (version 9.08, Cambridge Electronic Design). Average Vm of cortical neurons in the different periods of interest was calculated as the mean of the distribution of spontaneous subthreshold membrane potential fluctuations. Repetitive negative current pulses (200 ms duration, every 1 s, $n \geq 10$ trials per intensity) of increasing intensity (from −0.2 to −0.8 nA) were injected into cortical cells to calculate membrane

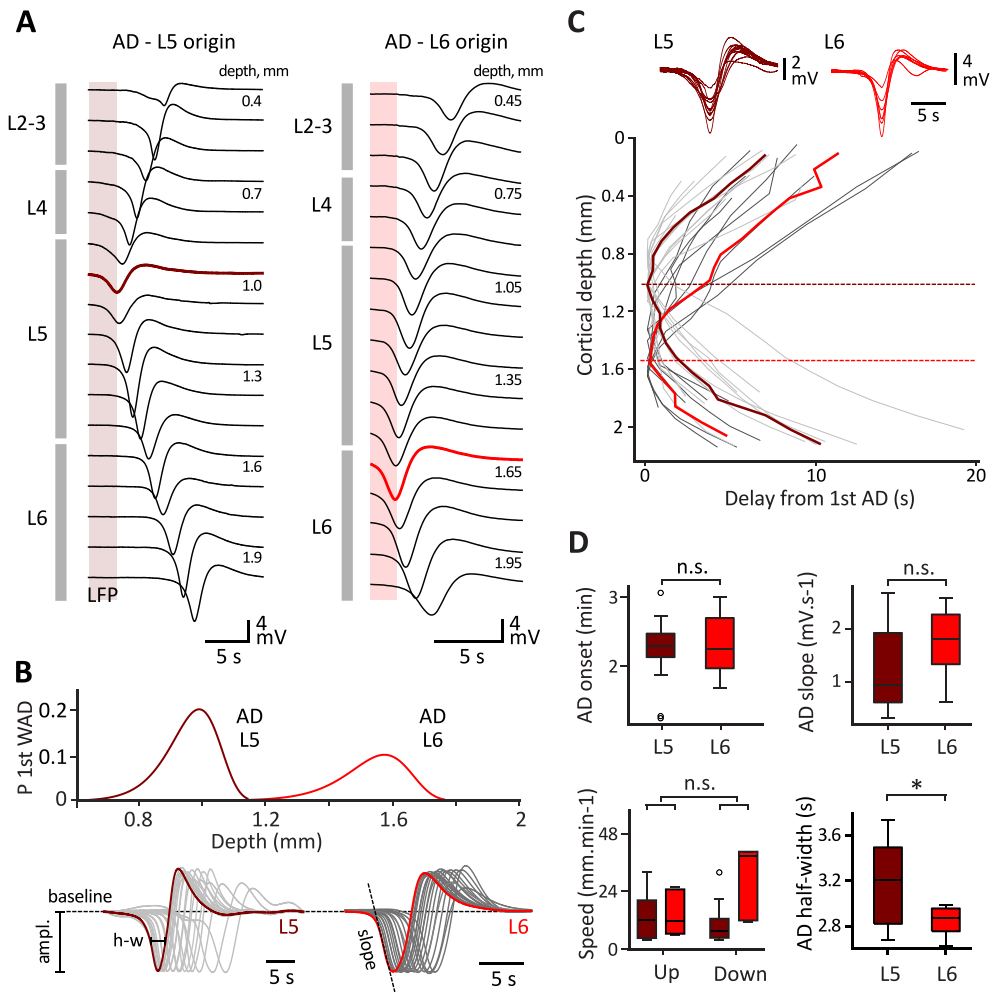

Fig. 3. Initiation and propagation of AD in S1. (A) Multilayer LFP recordings (32-channel silicone probe, 100 µm vertical separation distance between two electrodes) from two experiments showing that AD could be initiated in L5 (left, burgundy trace) or in L6 (right, red trace), before being bidirectionally propagated within the cortical column. Color-coded rectangles mark the time of the first AD. (B) Probability density (Weibull distribution) of AD initiation depths (top) ($n = 24$ protocols). Note the bimodal pattern indicating the two preferential initiation sites. Bottom: ADs recorded at the different depths in (A) were superimposed and their amplitude normalized to the first initiated AD (colored traces). AD amplitude (ampl.), half-width duration (h-w) and slope were measured on the first initial negative component as indicated. (C) AD onset times as a function of cortical depth ($n = 24$ protocols). The red and burgundy lines respectively represent the mean propagation profile of ADs initiated in L5 (light grey curves, $n = 16$) and L6 (dark grey curves, $n = 8$). The inset shows the superposition of the corresponding first ADs. (D) Boxplots comparing the slope of first ADs originating from L5 or L6, their time of occurrence as a function of Vent. off., upward and downward propagation speeds, and half-width durations. ns: non-significant; *: $P < 0.05$. (For interpretation of the references to color in this figure legend, the reader is referred to the web version of this article.)

input resistance (Rin). Measurements of voltage drops (averaged for each intensity) were made at the end of the membrane capacitance charge. Corresponding voltage-current (V—I) plots were constructed, and mean Rin values were calculated as the slope of the linear portion of V—I relations.

Amplitude of intracellular ADs and *DC* potential shifts was respectively calculated as the voltage difference between baseline Vm (measured on a 30-s period before Vent. off) and the onset of the AD plateau, or the first negative peak of the *DC* component (Fig. 5B and C). Onset latency of ADs and *DC* potentials was the time between Vent. off and the beginning of the AD plateau, or the first negative peak of the *DC* waveform.

2.6. Ouabain injections

Small volumes (50–100 nl) of 1–5 mM ouabain (Merck Millipore), a potent antagonist of Na^+-K^+ ATPases (Lingrel, 1992), or phosphate-buffered saline (PBS; vehicle experiments) were stereotaxically injected into S1 L2–3 (322 ± 3 µm, $n = 6$ experiments) or L5 (1012 ± 9 µm, $n = 6$ experiments), using calibrated glass micropipettes secured to a 10-µl Hamilton syringe, and positioned 250 µm lateral to the silicone probe. Injections were performed at a rate of 50 nl/s after observing a control period ≥15 min.

2.7. Statistical analysis

Statistical analysis was performed with MATLAB and SigmaStat v4.0 (Systat Software Inc.). Differences between groups were assessed using paired *t*-test, Wilcoxon signed-rank test, Mann-Whitney rank-sum test or ANOVA when appropriate. Correlations were evaluated by means of Pearson's r^2 values or Spearman's rho values. The sequential rejective Benjamini-Hochberg test procedure was used to correct for multiple comparisons (Benjamini and Hochberg, 1995). Results are represented as mean ± SD (unless stated otherwise) and the level of significance was set at $P < 0.05$.

3. Results

3.1. ECoG patterns during transient anoxia

The consequences of transient anoxia were first examined by monitoring vital signs and S1 ECoG activity in sufentanil-sedated rats subjected to 2–3 min of asphyxia (n = 10 experiments from 10 rats) (Fig. 1A). Asphyxia onset (Vent. off) resulted in an abrupt drop of $EtCO_2$ and a more gradual reduction of SpO_2. ECoG waveforms remained relatively unchanged for about 10 s before undergoing a global attenuation, interrupted by a transient episode of slow oscillations associated with an increase in signal amplitude (Fig. 1A, arrow). The low-frequency activity period was correlated with a significant slowing of the heart rate and the establishment of an anoxic state, associated with undetectable values of SpO_2 (13–63 s after asphyxia onset) (Fig. 1A and B, middle graph). The amplitude of the ECG signal then decreased rapidly to <10% of its control value, marking the onset of the isoelectric state (55.3 ± 23.3 s after Vent. off, n = 10 protocols) (Fig. 1A and B, left). The isoelectric state was maintained until the occurrence of a characteristic ECoG wave (termed here 'wave of anoxic depolarization', WAD), 128.4 ± 21.4 s after the onset of asphyxia (Fig. 1A and B, left). We previously showed in a comparable experimental model of asphyxia that WAD onset is accompanied by a nonreactive mydriasis (Schramm et al., 2020), indicative of the loss of brainstem functions. Restoration of oxygenation just after the WAD (see Methods) resulted in a fast return of $EtCO_2$ and a slow recovery of SpO_2 values (Fig. 1A). In the vast majority of cases (9 out of 10 protocols), reoxygenation caused the emergence of a post-anoxic ECoG wave (termed here 'wave of post-anoxic repolarization, WpAR), which systematically heralded the return of cortical activities and recovery of control values of heart rate (Fig. 1A and B, left and middle graphs). On average, ECoG amplitude and SpO_2 level fully recovered their normoxic values about one hour after Vent. on (Fig. 1A and B, right).

3.2. Laminar organization of anoxic cortical activities

To investigate the spatiotemporal properties of anoxia-induced cortical activities along the vertical axis of the cortical column, we performed large-scale LFP recordings using linear multisite electrodes inserted into the depth of S1. Layer boundaries were defined based on post-hoc analysis of NeuN immunofluorescence scan images showing the distribution of cortical neurons (see Supplementary Methods and Supplementary Fig. 2). Fig. 2A illustrates the activity patterns typically collected in the different cortical layers in control and after interruption of mechanical ventilation. As already reported for cortical surface recordings in other rat models of anoxia (Borjigin et al., 2013; Schramm et al., 2020) (see also Fig. 1A), spectral analysis of LFP signals revealed three main periods of changes in the frequency content of cortical activities, which were conserved across all recording sites in all experiments (n = 27 protocols from 16 rats) (Fig. 2A and B, top records). After a short period during which LFP activities retained normal amplitude and frequency, we observed a brief increase in the relative power of beta-gamma oscillations (15–40 Hz), whose mean latency across layers peaked at 20.5 ± 7.4 s after Vent. off (Fig. 2B). Paralleling ECoG changes, the second period was characterized by a decrease in frequency of LFP signals, which were then dominated by delta waves (0.5–5 Hz) mixed with theta-alpha oscillations (6–10 Hz). Averaging the maximum frequency power of theta-alpha and delta oscillations along the S1 column (see Methods) gave a mean onset time of 40.9 ± 17.3 s and 44.6 ± 12.6 s (n = 27 protocols), respectively. This increase in slow activity was followed by the establishment of an isoelectric state around a minute after Vent. off (57.0 ± 23.2 s) (Fig. 2B). Notably, the timing of the successive states of activity, as well as the onset of the isoelectric state, occurred in a relatively synchronous manner along the cortical column (P > 0.05 for each interlaminar comparison, ANOVA) (Fig. 2B, bottom graph). The power of delta oscillations, relative to the corresponding normoxic values, was however greater in L5–6 than in L2–3 (L5–6: 3.6 ± 4.1 *vs.* L2–3: 2.5 ± 2.3 times the baseline value, n = 27 protocols; P = 0.03, Wilcoxon signed-rank test), whereas the amplitude of the remaining frequency bands did not significantly differ between layers (n = 27 protocols; P > 0.2 for theta-alpha and beta-gamma bands, Wilcoxon signed-rank test) (Fig. 2A and C).

By means of simultaneous ECoG and intracellular recordings of S1 L5 pyramidal neurons, we characterized the neural correlates of the cortical states, defined on the frequency content of ECoG signals (Fig. 2D). Recorded cells had the typical morphological and electrophysiological features of deep layer pyramidal neurons (Altwegg-Boussac et al., 2014; Mahon and Charpier, 2012; Schramm et al., 2020), including a mean Vm of −65.7 ± 4.3 mV (n = 5 neurons from 5 rats), a normoxic spontaneous firing rate of 9.1 ± 5.6 Hz and regular spiking or intrinsic bursting current-evoked firing patterns (Fig. 2D, Norm.). The high-frequency activity period was associated with a slight membrane depolarization (Vm = −63.2 ± 3.2 mV, n = 5 neurons; P = 0.02, paired t-test) and a transient (12.6 ± 5.8 s) increase in cell firing (17.7 ± 18.4 Hz, 40% of increase, n = 5 neurons), as compared to normoxic condition (Fig. 2D, panel b). The fast and small Vm fluctuations characterizing the high-frequency cortical state were then replaced by large-amplitude slow depolarizations, accompanied by a hyperpolarized Vm (−68.2 ± 5.4 mV, n = 5 neurons; P = 0.02, paired t-test) and a significant attenuation of spontaneous firing (1.5 ± 1.4 Hz, n = 5 neurons; P = 0.02, paired t-test) (Fig. 2D, panel c). The entry in the isoelectric state coincided with the cessation of spontaneous firing and the loss of ECoG and Vm fluctuations (Fig. 2D) (see also Schramm et al., 2020).

3.3. Spatiotemporal properties of LFP ADs and pARs

The measure of AD onset times across layers led to the identification of two preferential sites of initiation, located in L5 (1065 ± 163 μm, n = 16 out of 24 protocols) and, to a lesser extent, in L6 (1520 ± 144 μm, n = 8 out of 24 protocols) (Fig. 3A-C). Intracortical ADs were initiated within 2–3 min after asphyxia onset and mostly displayed a biphasic shape characterized by an initial large negative voltage shift followed by a smaller positive component (Fig. 3A-D), as typically observed in high-pass filtering recording conditions (van Rijn et al., 2011; Zandt et al., 2011; Dreier et al., 2017). Onset time, slope and amplitude of the first occurring ADs did not significantly differ between the two initiation sites (n = 24 protocols; P = 0.98, 0.3 and 0.1, respectively, Mann-Whitney rank-sum test) (Fig. 3B and D). However, we found that the half-width duration of ADs initiated in L5 was significantly longer compared to those arising from L6 (L5: 3.2 ± 0.4 s, n = 24 protocols *vs.* L6: 2.8 ± 0.1, n = 24 protocols; P = 0.04, Mann-Whitney rank-sum test) (Fig. 3B and D), suggesting possible laminar differences in the profile of extracellular K^+ rise and/or in its buffering by glial cells. ADs from either L5 or L6 had a curvilinear bidirectional propagation profile toward the pia and corpus callosum (Fig. 3A and C). Despite relatively higher values of propagation speed in the downward direction when initiated from L6 (see Fig. 3A), the average propagation velocities were not significantly different between initiation sites (L5 → Up: 18.6 ± 15.9 mm.min^{-1}, n = 24 protocols *vs.* L 6 → Up: 13.9 ± 8.7 mm.min $^{-1}$, n = 24 protocols; P = 0.5, Mann-Whitney rank-sum test; L5 → Down: 13.0 ± 9.6 mm.min $^{-1}$, n = 24 protocols *vs.* L6 → Down: 32.8 ± 18.6 mm.min $^{-1}$, n = 24 protocols; P = 0.14, Mann-Whitney rank-sum test) (Fig. 3C and D). Overall, the time required for systemic anoxia to depolarize the entire S1 cortical column was 9.4 ± 5.8 s (n = 24 protocols) (Fig. 3D). Comparison of AD properties in animals subjected to two successive anoxia protocols (separated by a recovery period ≥80 min, see Methods) did not reveal significant differences between sessions (P > 0.4 for each parameter, Mann-Whitney rank-sum test) (Supplementary Fig. 3), indicating that initial exposure to transient anoxia did not induce persistent cellular and metabolic defects interfering with our measurements.

We next sought to determine whether the characteristic post-anoxic wave that followed the return of oxygen supply exhibited a particular

spatiotemporal pattern within S1. We found that brain re-oxygenation after the last detected AD in the multisite LFPs could trigger post-anoxic waves of repolarization (pARs) throughout the vertical axis of the cortical column (Fig. 4A). The shape of pARs was also globally biphasic, but with a greater shape variability and a reversed polarity compared to LFP ADs, as expected if ADs and pARs respectively reflect Vm depolarization and repolarization of neocortical neurons (Fig. 4A,B and Fig. 5B, C) (see also Schramm et al., 2020). The timing of the first LFP pAR within the cortical column was highly variable (from 10.5 to 40.2 s after Vent. on, mean = 17.7 ± 7 s, n = 24 protocols), regardless of the AD initiation site (L5 or L6, $P = 0.19$). As shown by the broad distribution of the origin depth of pARs, we could not detect a preferential site of emergence for the post-anoxic wave (Fig. 4B, bottom). Accordingly, there was no correlation between the origin site of LFP ADs and that of LFP pARs ($n = 24$ protocols; Spearman's $r_s = -0.07$, $P = 0.74$) (Fig. 4C). Finally, the timing of the pARs recorded at different depths within the cortical column, relative to the first post-anoxic wave, did not show any specific pattern that may suggest a propagation process (Fig. 4D).

3.4. Neuronal substrates of anoxic waves

The multisite LFP recordings suggested that cortical neurons from the deep layers could be the first to depolarize during anoxia. To directly unveil the sequence of neuronal depolarizations within the cortical column, we first performed double *DC* recordings with glass micropipettes inserted in infra- and supragranular layers ($n = 12$ protocols from 4 rats). As previously reported (Somjen, 2004; Schramm et al., 2020; Charpier, 2023), the *DC* shifts observed at different depths after oxygen deprivation exhibited the characteristics of cellular ADs when recorded from the extracellular space (Fig. 5A and B). Deep and superficial *DC* shifts displayed similar amplitude and the slope of their initial negative deflection was also not significantly different ($P > 0.05$ for both parameters, Mann-Whitney rank-sum test) (Fig. 5D). Applying off-line the LFP filtering parameters (between 0.1 Hz and 6 kHz) to the *DC* potentials resulted in signals whose shape reliably reproduced the ADs and pARs as recorded with silicon probes (Fig. 5B), demonstrating the identity between *DC* shifts and the anoxia-related LFP waves. Furthermore, as consistently observed with LFP ADs, anoxia-induced *DC* shifts in L5 systematically preceded by 3 to 16 s (7.3 ± 4 s, $n = 12$ protocols) those

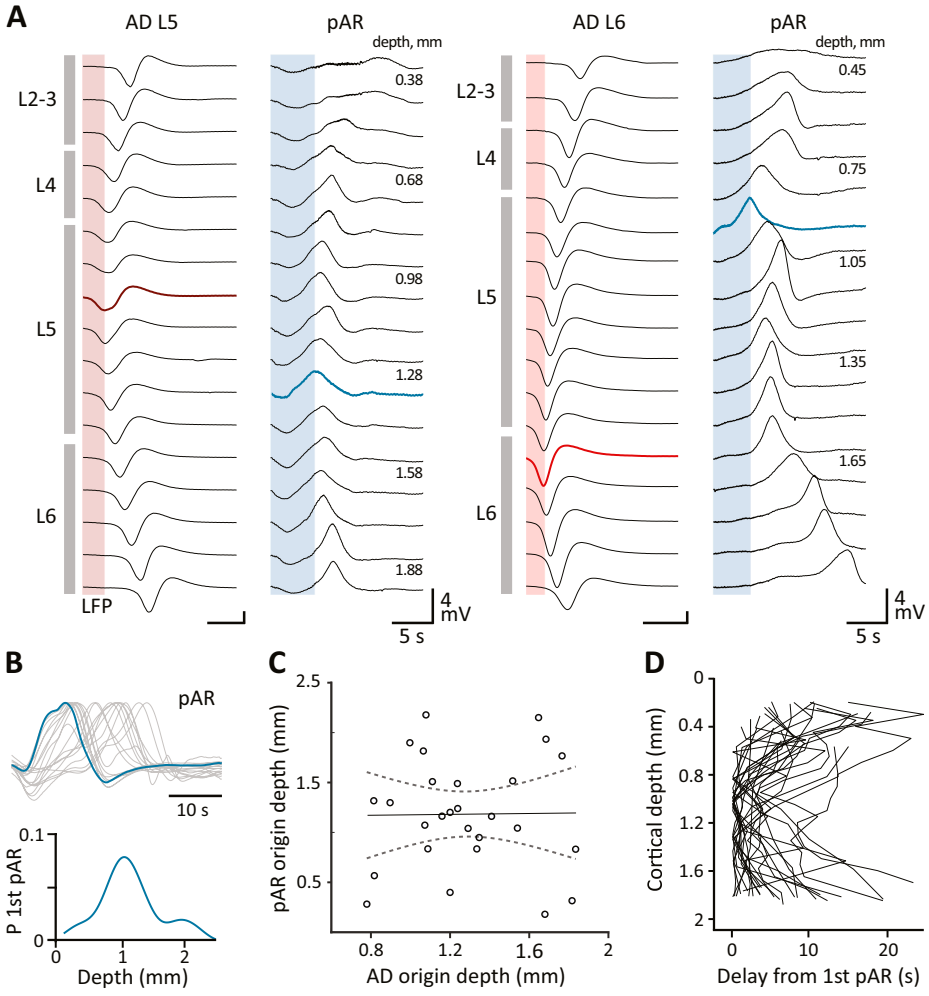

Fig. 4. Spatiotemporal dynamics of pARs. (A) Typical LFP recordings (32-channel silicone probe, 100 μm vertical separation distance between two electrodes) from two experiments showing the layer-related temporal profile of pARs, when the corresponding AD was initiated in L5 (left) or in L6 (right). The first ADs and pARs are in red/burgundy and blue, respectively. Color-coded rectangles mark the time of first ADs and pARs. (B) Superimposition of pARs after normalization of their amplitude to the first pAR (blue trace). Bottom: Density probability (kernel smoothing) of the first pARs as a function of cortical depth ($n = 24$ protocols). (C) Scatter plot of pARs origin depth as a function of the initiation depth of the corresponding ADs. Linear fit (black line) and 95% confidence interval (grey dashed lines) are illustrated (Spearman's $r_s = -0.07$; $P = 0.74$). (D) Group data of pARs timings (relative to the first pAR) as a function of cortical depth ($n = 24$ protocols). (For interpretation of the references to color in this figure legend, the reader is referred to the web version of this article.)

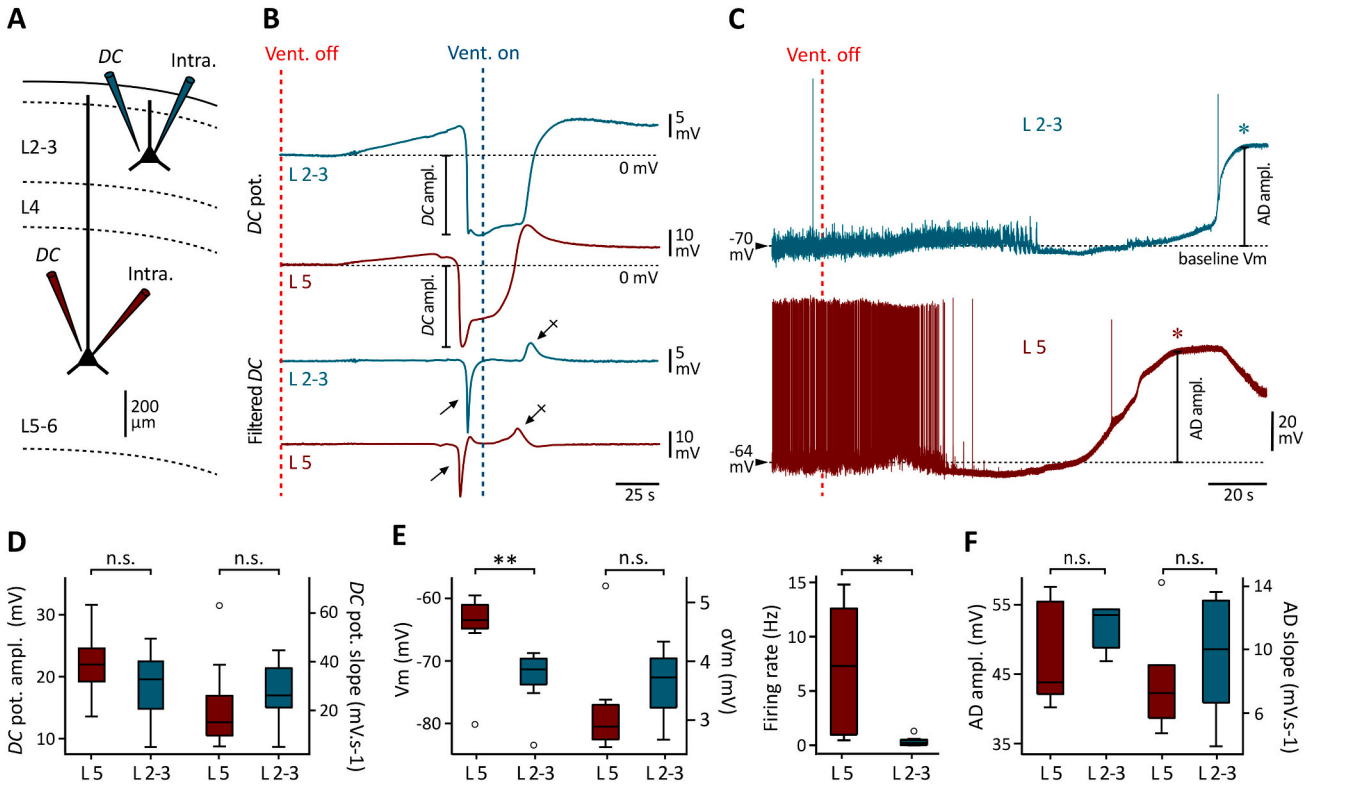

Fig. 5. Neuronal correlates of LFP ADs. (A) Simultaneous *DC* recordings, using NaCl-filled electrodes, were made from S1 L2–3 and L5. In separate experiments, intracellular recordings were performed at the same depths. (B) Typical anoxia-induced *DC* shifts (top records) recorded conjointly at the indicated location, after anoxia onset (Vent. off) and following restoration of the ventilation (Vent. on). The amplitude of *DC* potentials (*DC* ampl.) was computed as indicated. The bottom traces are the corresponding filtered signals (0.1 Hz – 6 kHz). Note that the initial (arrows) and terminal (crossed arrows) deflections of filtered records display shapes reminiscent of ADs and pARs recorded with silicon probes. (C) Intracellular activity of pyramidal cells located in superficial (L2–3) and deep (L5) layers, before and after interruption of artificial ventilation. AD amplitude was measured between baseline Vm and the onset of the AD plateau (asterisk). The time at which ventilation was restored has been omitted for clarity. (D) Pooled data comparing the amplitude and the initial slope of *DC* potentials recorded from L2–3 ($n = 12$) and L5 ($n = 12$). (E) Mean Vm, standard deviation of Vm (σVm) and spontaneous firing rate, measured from pyramidal neurons located in superficial ($n = 8$) and deep ($n = 10$) layers. (F) Comparison of AD amplitude and slope measured from L2–3 ($n = 5$) and L5 ($n = 5$) pyramidal neurons. ** $P < 0.01$, * $P < 0.05$, n.s.: non-significant.

in upper layers, corresponding to an average propagation velocity (14.3 ± 9.3 mm.min $^{-1}$, $n = 12$ protocols) comparable to that measured with silicon probes ($P = 0.74$, Mann-Whitney rank-sum test).

To further characterize the neuronal correlates of LFP ADs and determine the electrophysiological properties of cortical neurons responsible for their initiation, we performed intracellular recordings from pyramidal neurons located in L5 ($n = 10$ from 5 rats) or L2–3 ($n = 8$ from 5 rats) in normoxic condition, and during the anoxic procedure (Fig. 5A). In control condition, deep-layer neurons were significantly more depolarized (L5: −65.1 ± 6.2 mV, $n = 10$) than their superficial counterparts (L2–3: −72.8 ± 4.8 mV, $n = 8$; $P = 0.006$, Mann-Whitney rank-sum test) and displayed a higher firing rate (L5: 6.9 ± 5.9 Hz, $n = 10$ *vs.* L2–3: 0.3 ± 0.5 Hz, $n = 8$; $P = 0.011$, Mann-Whitney rank-sum test), whereas the amplitude of Vm fluctuations, reflecting the amount of background synaptic activity (Altwegg-Boussac et al., 2014), was similar between the two cell groups ($P > 0.05$, Mann-Whitney rank-sum test) (Fig. 5C and E). Because Rin of deep and superficial neurons (L5, 25.0 ± 9.7 MΩ, $n = 5$ *vs.* L2–3, 23.2 ± 11.1 MΩ, $n = 5$; $P = 0.9$, Mann-Whitney rank-sum test), as well as their voltage firing threshold (L5, −52.4 ± 4.3 mV, $n = 8$ *vs.* L2–3, −54.4 ± 4.9 mV, $n = 5$; $P = 0.5$, Mann-Whitney rank-sum test) were not statistically different, it is likely that the exacerbated spiking activity in L5–6 neurons was primarily due to their relative membrane depolarization (Lefort et al., 2009). In ten experiments (from 10 rats), L5 and L2–3 neurons could be intracellularly recorded throughout the anoxic process up to the occurrence of AD. In agreement with *DC* and LFP experiments, the mean latency (as a function of Vent. Off) of AD plateau onsets was shorter in L5 (129.0 ± 26.2 s, $n = 5$ neurons) than in L2–3 neurons (141.0 ± 16.2 s, $n = 5$ neurons). However, the magnitude of the depolarizing plateau and maximal slope of the intracellular AD were comparable in both neuronal populations ($P = 0.69$ and $P = 0.55$, Mann-Whitney rank-sum test) (Fig. 5F).

3.5. Local blockade of ATPases reproduces AD dynamics

Our results show that L5 pyramidal neurons are more likely to initiate and propagate AD during systemic anoxia. As deep-layer pyramidal cells were found to be more depolarized and active than their superficial counterparts, the elevated proneness of L5 to AD could result from a higher metabolic demand and, thus, a greater vulnerability to ATP deprivation (Attwell and Laughlin, 2001; Hallermann et al., 2012; Shetty et al., 2012). To explore the role of Na^+-K^+ ATPases in AD initiation, we coupled silicon probe recordings in S1 with layer-specific injections of ouabain, a Na^+-K^+ ATPase blocker known to elicit spreading anoxic-like depolarizations *in vitro* (Balestrino et al., 1999; Pietrobon and Moskowitz, 2014). Intracortical injection of ouabain in L2–3 or L5 led to the emergence of biphasic LFP potentials (ouabain-induced depolarizations, ODs) whose morphology was closely similar to that of ADs (Fig. 6A and B). The first ODs occurred close to the corresponding superficial ($n = 6$ protocols from 6 rats) or deep ($n = 6$ protocols from 6 rats) injection sites (Fig. 6A and D) and had similar delays relative to the time of injection ($P = 0.9$, Mann-Whitney rank-sum test) (Fig. 6E), indicating that the ATPase blocker had a spatially limited effect. Similar local injections of small volumes of PBS did not induce any changes in local LFP activity. Half-width duration and maximum slope

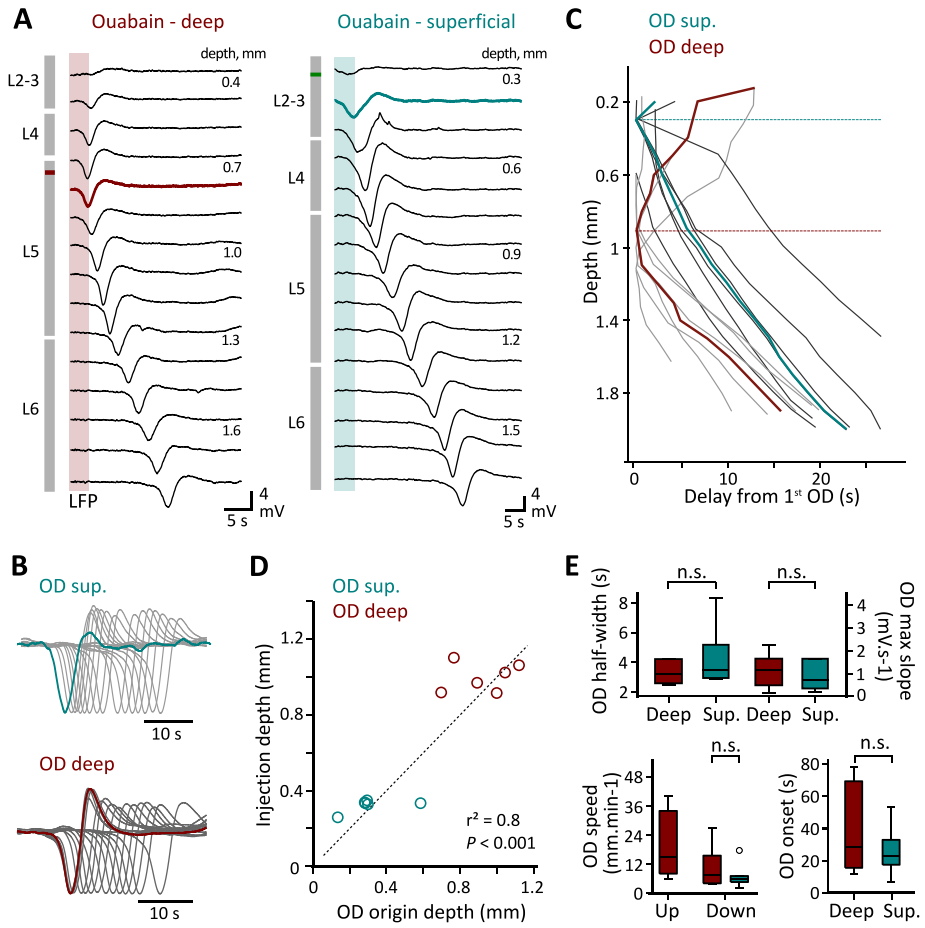

Fig. 6. Properties of ouabain-induced depolarizations in S1. (A) Laminar profile of ouabain-induced depolarizations (ODs) after focal injection (indicated by the color-coded marks) of the ATPase blocker in L5 (left, deep injection) or L2–3 (right). Color-coded rectangles mark the time of the first OD. LFP activities were recorded with a 32-channel silicone probe (100 µm vertical separation distance between two electrodes). (B) Superposition of the ODs shown in (A). Recordings are normalized to the amplitude of the first ODs (red or blue-green traces). (C) Depth-dependent origin of the ODs and their vertical spread within the cortical column. The red and blue-green lines represent the average propagation profile of ODs initiated in L5 (light grey curves, $n = 6$ experiments) and L2–3 (dark grey curves, $n = 6$ experiments). (D) Relationship between the location of ouabain injection site and the depth of OD first occurrence. The black dashed line represents the equivalence line. (E) Group data comparing the slope and half-width duration values of first ODs elicited in deep (red) and superficial (blue-green) layers (top), their propagation velocities in both directions (the upward propagation speed in the case of superficial injections has been omitted), and their onset latency as a function of the injection time. ns: non-significant. ns: non-significant; *: $P < 0.05$. (For interpretation of the references to color in this figure legend, the reader is referred to the web version of this article.)

of the first negative LFP shift (Fig. 6B and E) were also comparable between ODs generated in the deep ($n = 6$ protocols) or superficial layers ($n = 6$ protocols) (half-width duration, $P = 0.4$; maximum slope, $P = 0.9$, Mann-Whitney rank-sum test). Superficially- and deeply-initiated ODs spread vertically with similar velocities (L2–3, 7.3 ± 5.4 mm.min^{-1}, $n = 6$ protocols *vs.* L5, 10.9 ± 9.1 mm.min^{-1}, $n = 6$ protocols; $P = 0.8$, Mann-Whitney rank-sum test) (Fig. 6E), and their spatiotemporal propagation profile was strongly reminiscent of that obtained during systemic anoxia (Fig. 6C). Interestingly, when OD and AD properties were compared, we did not find significant differences in their amplitude, negative slope, half-width duration, and propagation velocity (Supplementary Fig. 4), suggesting that both types of waves were underpinned by similar basic cellular mechanisms and follow the same propagation process.

4. Discussion

We have examined how cortical activities are modified and structured in the different layers of S1 during anoxia. Common to all layers was the succession, in the early phase of asphyxia, of three stereotyped patterns of activity: a bump of high-frequency activity followed by an episode of low-frequency oscillations ending in a sustained period of electrical silence. However, the cortical layers differed in their proneness to AD, which was predominantly initiated by a subset of deep-layer neurons highly vulnerable to anoxia. We also observed that AD could be reversed by the restoration of normal metabolic conditions and showed that post-anoxic waves, reflecting the repolarization of cortical neurons, could reliably predict the recovery of brain activity after anoxia.

4.1. Possible mechanisms for the stereotyped cortical patterns preceding AD

High-frequency oscillations, resembling in amplitude and frequency the cortical activity encountered during wakefulness (Steriade et al., 2001), have been already observed in other rodent models of global anoxia induced by cardiac arrest (Borjigin et al., 2013), decapitation (Kongara et al., 2014) or asphyxia (Schramm et al., 2020). They have also been detected after terminal extubation in the EEG of patients undergoing a do-not-resuscitate and comfort care protocol (Vicente et al., 2022; Xu et al., 2023), and have been proposed to support the sensory perceptions associated with near-death experiences (Van Lommel et al., 2001; Borjigin et al., 2013). Performing combined surface and

intracellular recordings, we found that fast ECoG activities correlated with low amplitude, high-frequency Vm fluctuations and repetitive firing in pyramidal cells. This peculiar synaptic activity could arise from an overactivation of synaptic receptors, due to an excessive release of glutamate in the interstitial medium, as observed *in vitro* in S1 L5 and CA1 hippocampal neurons during the first minute of hypoxia (Katchman and Hershkowitz, 1993; Fleidervish et al., 2001; Pietrobon and Moskowitz, 2014).

Cortical pyramidal neurons mostly displayed slowly developing subthreshold synaptic depolarizations during the subsequent low-frequency cortical pattern. Although the cellular underpinnings of this anoxia-induced slow cortical state are not yet fully understood, *in vitro* investigations suggest that it could result from subtle interactions between ATP-sensitive K^+ channels and recurrent excitatory synaptic activity within the cortical network (Cunningham et al., 2006). Consistently, a recent neural network model predicted that hypometabolic conditions should lead to a decrease in neuronal firing activity and trigger an oscillatory pattern that would progressively synchronize at delta frequency with the further decline in ATP production (Joo et al., 2021). The slowing of cortical waveforms was systematically followed by a dissolution of neuronal and synaptic activity, causing an isoelectric state at intracellular, LFP and ECoG levels (Xu and Pulsinelli, 1996; Schramm et al., 2020). This may result from multiple mechanisms depressing synaptic transmission, such as a reduction of presynaptic Ca^{2+} currents and/or partial failure of presynaptic AP conduction (Young and Somjen, 1992). The concomitance of cortical states across layers suggests a spatially homogeneous depletion of ATP stores during the first minute of anoxia and the activation of the synaptic and intrinsic mechanisms described above with similar kinetics. The early period of the dying process thus contrasts sharply with the depth-dependent properties of AD.

4.2. Laminar-specific vulnerability to AD

Previous studies have interrogated the heterogenous incidence of AD across cortical areas and layers. Leão was the first to show that AD induced in the rabbit by carotid arteries occlusion did not develop simultaneously in all regions of the cerebral hemisphere and that superficial cortical layers were highly sensitive to anoxia (Leão, 1947; Leão and Morison, 1945). Later *in vivo* and *in vitro* works led to contradictory results, with AD being initiated in the supragranular (Basarsky et al., 1998; Jarvis et al., 2001; Joshi and Andrew, 2001; Kaufmann et al., 2017), granular (Juzekaeva et al., 2017) or infragranular (Richter and Lehmenkühler, 1993) layers, depending on the experimental conditions and stimuli used to induce AD. We revisited this issue *in vivo* with the combination of multisite LFP, *DC* and intracellular recordings, which, to our knowledge, has not been yet been applied to systemic anoxia. Our LFP recordings revealed that AD preferentially originated from L5, and to a lesser extent from L6, before slowly spreading in a bidirectional manner to the rest of the column. This high proneness of L5 to AD was confirmed by *DC* and intracellular recordings in L2–3 and L5, which showed a greater probability of deep-layer pyramidal neurons to depolarize before their superficial counterparts. We also demonstrated that focal injection of small volumes of ouabain within a specific cortical layer rapidly triggered cortical waves whose shape, amplitude and propagation profile were highly similar to ADs. ODs first arose close to the injection site, demonstrating that blockade of Na^+-K^+ ATPases in a restricted region of the cortex is sufficient to reproduce the spatiotemporal dynamics of LFP AD induced by global anoxia. These results strongly suggest a crucial role for ATPase pumps and the loss of transmembrane electrochemical gradients in the initiation and propagation of the anoxic process. These findings are in line with the general assumption that the self-regenerating membrane depolarization induced by the failure of Na^+-K^+ ATPases ultimately leads to a massive increase in the extracellular K^+ level, whose diffusion into the interstitial medium promotes the slow propagation of AD (Somjen, 2001; Pietrobon and Moskowitz, 2014).

Several non-exclusive phenomena could participate to the rising of K^+ in a particular cortical region. A high level of activity in a subpopulation of neurons, locally increasing metabolic demand and vulnerability to depletion of ATP reserves, could promote AD initiation. Consistent with their strong synaptic coupling with other nearby excitatory neurons and in agreement with previous investigations (Lefort et al., 2009; O'Connor et al., 2010; Oberlaender et al., 2012), we found that L5 neurons displayed a more depolarized membrane potential than L2/3 neurons and a much higher spontaneous firing rate. These properties of L5 neurons might endow these neurons with higher metabolic needs and increase their proneness to initiate waves of depolarization when submitted to anoxic conditions. Interestingly, an increase in extracellular K^+ concentration or temperature, two conditions thought to promote neuronal firing (Reig et al., 2009; Zandt et al., 2011), has been shown to accelerate AD onset *in vitro* (Jarvis et al., 2001; Joshi and Andrew, 2001; Juzekaeva et al., 2017). A high neuronal density promoting mutual depolarization in cortical subnetworks has also been proposed as an additional mechanism to explain the differential sensitivity of cortical layers to anoxia (Juzekaeva et al., 2017). While this parameter is unlikely to contribute to the susceptibility of L5 neurons in the forelimb region where cell density is relatively low compared to adjacent L4 and L6 (Narayanan et al., 2017), it could participate to the high proneness of L6 to AD.

In >90% of cases, resuming artificial ventilation after a few minutes of asphyxia led to the appearance of a biphasic wave in the ECoG (WpAR) and LFP (pAR) records. We have previously shown that these waves reflect the repolarization of cortical neurons and heralds the return of synaptic and firing activity in cortical networks (Schramm et al., 2020; present study). It is believed that brain re-oxygenation initiates the reconstitution of ATP stores and reactivation of neuronal and glial Na^+-K^+ ATPase which, by buffering the extracellular K^+ in excess, allows the gradual re-establishment of electrochemical gradients and repolarization of neuronal membranes. This repolarization was identified in the present study as a positive variation in the *DC* shift in both superficial and infragranular layers. Multisite recordings indicate that LFP pARs did not show any particular spatiotemporal profile in the cortical column, demonstrating that post-anoxic recovery of membrane polarization is not a propagated process. The restoration of ion homeostasis could rather be dominated by structural and/or functional constraints such as the local density of glial cells or the level of Na^+-K^+ ATPase activity, which has been shown to vary within the population of cortical neurons (Anderson et al., 2010).

5. Conclusions

Our study provides evidence that the initial phase of anoxia is associated with a set of stereotyped changes in cortical neurons and networks, which undergo a substantial increase in activity before gradually declining and stopping. Unlike these early alterations, which occur almost synchronously in all cortical layers, AD is initiated locally by a subset of neurons in the deep layers before spreading to the rest of the cortical column. We have identified the disruption of Na^+-K^+ ATPases, leading to the loss of transmembrane electrochemical gradients, as a key event in the focal initiation of AD. An elevated metabolic demand, resulting from a high firing rate of pyramidal neurons in L5, could contribute to the increased susceptibility of this layer to ATP depletion and its high propensity to AD. A more detailed understanding of the mechanisms underlying the heterogeneous vulnerability to anoxia of different populations of cortical neurons appears to be a major challenge for future research, as it would ultimately offer the possibility to identify drugs or neuroprotective strategies capable of interfering with AD, either directly at the site of initiation or by limiting its propagation.

Funding

This work was supported by Sorbonne Université (Emergence-2019), the Agence Nationale de la Recherche (ANR-10- IAIHU-06), and the Institut National de la Santé et de la Recherche Médicale (Inserm). Animals were housed in the PHENO-ICMice core facility, which is supported by 2 Investissements d'avenir (ANR-10- IAIHU-06 and ANR-11-INBS-0011- NeurATRIS) and the Fondation pour la Recherche Médicale.

CRediT authorship contribution statement

Antoine Carton-Leclercq: Methodology, Validation, Investigation, Data curation, Formal analysis, Visualization, Writing – review & editing. **Sofia Carrion-Falgarona:** Investigation, Formal analysis, Writing – review & editing. **Paul Baudin:** Formal analysis, Writing – review & editing. **Pierre Lemaire:** Investigation, Formal analysis. **Sarah Lecas:** Formal analysis, Writing – review & editing. **Thomas Topilko:** Formal analysis. **Stéphane Charpier:** Conceptualization, Methodology, Validation, Writing – original draft, Supervision, Funding acquisition. **Séverine Mahon:** Conceptualization, Methodology, Validation, Writing – original draft, Formal analysis, Visualization, Supervision, Funding acquisition.

Declaration of Competing Interest

The authors report no competing interests.

Data availability

The data that support the findings of this study are available from the corresponding author, upon reasonable request.

Appendix A. Supplementary data

Supplementary data to this article can be found online at https://doi.org/10.1016/j.nbd.2023.106345.

References

Altwegg-Boussac, T., Chavez, M., Mahon, S., Charpier, S., 2014. Excitability and responsiveness of rat barrel cortex neurons in the presence and absence of spontaneous synaptic activity in vivo. J. Physiol. 592 (16), 3577–3595. https://doi.org/10.1113/jphysiol.2013.270561.

Altwegg-Boussac, T., Schramm, A.E., Ballestero, J., Grosselin, F., Chavez, M., Lecas, S., Baulac, M., Naccache, L., Demeret, S., Navarro, V., Mahon, S., Charpier, S., 2017. Cortical neurons and networks are dormant but fully responsive during isoelectric brain state. Brain. 140 (9), 2381–2398. https://doi.org/10.1093/brain/awx175.

Anderson, T.R., Huguenard, J.R., Prince, D.A., 2010. Differential effects of Na+-K+ ATPase blockade on cortical layer V neurons. J. Physiol. 588 (22), 4401–4414. https://doi.org/10.1113/jphysiol.2010.191858.

Andrew, R.D., Hsieh, Y.T., Brisson, C.D., 2017. Spreading depolarization triggered by elevated potassium is weak or absent in the rodent lower brain. J. Cereb. Blood Flow Metab. 37 (5), 1735–1747. https://doi.org/10.1177/0271678X16657344.

Attwell, D., Laughlin, S.B., 2001. An energy budget for signaling in the grey matter of the brain. J. Cereb. Blood Flow Metab. 21 (10), 1133–1145. https://doi.org/10.1097/00004647-200110000-00001.

Balestrino, M., Young, J., Aitken, P., 1999. Block of (Na+,K+)ATPase with ouabain induces spreading depression-like depolarization in hippocampal slices. Brain Res. 838 (1–2), 37–44. https://doi.org/10.1016/S0006-8993(99)01674-1.

Basarsky, T.A., Duffy, S.N., Andrew, R.D., MacVicar, B.A., 1998. Imaging spreading depression and associated intracellular calcium waves in brain slices. J. Neurosci. 18 (18), 7189–7199. https://doi.org/10.1523/jneurosci.18-18-07189.1998.

Baudin, P., Whitmarsh, S., Cousyn, L., Roussel, D., Lecas, S., Lehongre, K., Charpier, S., Mahon, S., Navarro, V., 2022. Kv1.1 channels inhibition in the rat motor cortex recapitulates seizures associated with anti-LGI1 encephalitis. Prog. Neurobiol. 213 (November 2021) https://doi.org/10.1016/j.pneurobio.2022.102262.

Benjamini, Y., Hochberg, Y., 1995. Controlling the false discovery rate: a practical and powerful approach to multiple testing. J. R. Stat. Soc. Ser. B 57 (1), 289–300. https://doi.org/10.1111/j.2517-6161.1995.tb02031.x.

Bogdanov, V.B., Middleton, N.A., Theriot, J.J., Parker, P.D., Abdullah, O.M., Ju, Y.S., Hartings, J.A., Brennan, K.C., 2016. Susceptibility of primary sensory cortex to spreading depolarizations. J. Neurosci. 36 (17), 4733–4743. https://doi.org/10.1523/jneurosci.3694-15.2016.

Borjigin, J., Lee, U., Liu, T., Pal, D., Huff, S., Klarr, D., Sloboda, J., Hernandez, J., Wang, M.M., Mashour, G.A., 2013. Surge of neurophysiological coherence and connectivity in the dying brain. Proc. Natl. Acad. Sci. U. S. A. 110 (35), 14432–14437. https://doi.org/10.1073/pnas.1308285110.

Bruno, R.M., Sakmann, B., 2006. Cortex is driven by weak but synchronously active thalamocortical synapses. Science 312 (June), 1622–1627. https://doi.org/10.1126/science.1124593.

Charpier, S., 2023. Between life and death: the brain twilight zones. Front. Neurosci. May, 1–18. https://doi.org/10.3389/fnins.2023.1156368.

Clarke, D.D., Sokoloff, L., 1999. Circulation and energy metabolism of the brain. In: Lippincott-Raven, Siegel, G.J., Agranoff, B.W., Albers, R.W., Fisher, S.K., Uhler, M.D. (Eds.), Basic Neurochemistry: Molecular, Cellular and Medical Aspects, 6th Edition. New York, pp. 637–669.

Cunningham, M.O., Pervouchine, D.D., Racca, C., Kopell, N.J., Davies, C.H., Jones, R.S., Traub, R.D., Whittington, M.A., 2006. Neuronal metabolism governs cortical network response state. Proc. Natl. Acad. Sci. U. S. A. 103 (14), 5597–5601. https://doi.org/10.1073/pnas.0600604103.

Dreier, J.P., 2011. The role of spreading depression, spreading depolarization and spreading ischemia in neurological disease. Nat. Med. 17 (4), 439–447. https://doi.org/10.1038/nm.2333.

Dreier, J.P., Fabricius, M., Ayata, C., Sakowitz, O.W., Shuttleworth, C.W., Dohmen, C., Graf, R., Vajkoczy, P., Helbok, R., Suzuki, M., Schiefecker, A.J., Major, S., Winkler, M.K., Kang, E.J., Milakara, D., Oliveira-Ferreira, A.I., Reiffurth, C., Revankar, G.S., Sugimoto, K., Dengler, N.F., Hecht, N., Foreman, B., Feyen, B., Kondziella, D., Friberg, C.K., Piilgaard, H., Rosenthal, E.S., Westover, M.B., Maslarova, A., Santos, E., Hertle, D., Sánchez-Porras, R., Jewell, S.L., Balança, B., Platz, J., Hinzman, J.M., Lückl, J., Schoknecht, K., Schöll, M., Drenckhahn, C., Feuerstein, D., Eriksen, N., Horst, V., Bretz, J.S., Jahnke, P., Scheel, M., Bohner, G., Rostrup, E., Pakkenberg, B., Heinemann, U., Claassen, J., Carlson, A.P., Kowoll, C. M., Lublinsky, S., Chassidim, Y., Shelef, I., Friedman, A., Brinker, G., Reiner, M., Kirov, S.A., Andrew, R.D., Farkas, E., Güresir, E., Vatter, H., Chung, L.S., Brennan, K. C., Lieutaud, T., Marinesco, S., Maas, A.I., Sahuquillo, J., Dahlem, M.A., Richter, F., Herreras, O., Boutelle, M.G., Okonkwo, D.O., Bullock, M.R., Witte, O.W., Martus, P., van den Maagdenberg, A.M., Ferrari, M.D., Dijkhuizen, R.M., Shutter, L.A., Andaluz, N., Schulte, A.P., MacVicar, B., Watanabe, T., Woitzik, J., Lauritzen, M., Strong, A.J., Hartings, J.A., 2017. Recording, analysis, and interpretation of spreading depolarizations in neurointensive care: review and recommendations of the COSBID research group. J. Cereb. Blood Flow Metab. 37 (5), 1595–1625. https://doi.org/10.1177/0271678X16654496.

Fleidervish, I.A., Gebhardt, C., Astman, N., Gutnick, M.J., Heinemann, U., 2001. Enhanced spontaneous transmitter release is the earliest consequence of neocortical hypoxia that can explain the disruption of normal circuit function. J. Neurosci. 21 (13), 4600–4608. https://doi.org/10.1523/jneurosci.21-13-04600.2001.

Hallermann, S., De Kock, C.P.J., Stuart, G.J., Kole, M.H.P., 2012. State and location dependence of action potential metabolic cost in cortical pyramidal neurons. Nat. Neurosci. 15 (7), 1007–1014. https://doi.org/10.1038/nn.3132.

Hofmeijer, J., Van Putten, M.J.A.M., 2012. Ischemic cerebral damage: an appraisal of synaptic failure. Stroke. 43 (2), 607–615. https://doi.org/10.1161/STROKEAHA.111.632943.

Jarvis, C.R., Anderson, T.R., Andrew, R.D., 2001. Anoxic depolarization mediates acute damage independent of glutamate in neocortical brain slices. Cereb. Cortex 11 (3), 249–259. https://doi.org/10.1093/cercor/11.3.249.

Joo, P., Lee, H., Wang, S., Kim, S., Hudetz, A.G., 2021. Network model with reduced metabolic rate predicts spatial synchrony of neuronal activity. Front. Comput. Neurosci. 15 (October), 1–12. https://doi.org/10.3389/fncom.2021.738362.

Joshi, I., Andrew, R.D., 2001. Imaging anoxic depolarization during ischemia-like conditions in the mouse hemi-brain slice. J. Neurophysiol. 85 (1), 414–424. https://doi.org/10.1152/jn.2001.85.1.414.

Juzekaeva, E., Nasretdinov, A., Gainutdinov, A., Sintsov, M., Mukhtarov, M., Khazipov, R., 2017. Preferential initiation and spread of anoxic depolarization in layer 4 of rat barrel cortex. Front. Cell. Neurosci. 11 (December), 1–11. https://doi.org/10.3389/fncel.2017.00390.

Katchman, A.N., Hershkowitz, N., 1993. Early anoxia-induced vesicular glutamate release results from mobilization of calcium from intracellular stores. J. Neurophysiol. 70 (1), 1–7. https://doi.org/10.1152/jn.1993.70.1.1.

Kaufmann, D., Theriot, J.J., Zyuzin, J., Service CA, Chang, J.C., Tang, Y.T., Bogdanov, V. B., Multon, S., Schoenen, J., Ju, Y.S., Brennan, K.C., 2017. Heterogeneous incidence and propagation of spreading depolarizations. J. Cereb. Blood Flow Metab. 37 (5), 1748–1762. https://doi.org/10.1177/0271678X16659496.

Kongara, K., McIlhone, A.E., Kells, N.J., Johnson, C.B., 2014. Electroencephalographic evaluation of decapitation of the anaesthetized rat. Lab. Anim. 48 (1), 15–19. https://doi.org/10.1177/0023677213502016.

Leão, A.A.P., 1947. Further observations on the spreading depression of activity in the cerebral cortex. J. Neurophysiol. 10, 409–414.

Leão, A.A.P., Morison, R.S., 1945. Propagation of spreading cortical depression. J. Neurophysiol. 8 (1), 33–45.

Lefort, S., Tomm, C., Floyd Sarria, J.C., Petersen, C.C.H., 2009. The excitatory neuronal network of the C2 barrel column in mouse primary somatosensory cortex. Neuron. 61 (2), 301–316. https://doi.org/10.1016/j.neuron.2008.12.020.

Lingrel, J.B., 1992. Na,K-ATPase: isoform structure, function, and expression. J. Bioenerg. Biomembr. 24 (3), 263–270. https://doi.org/10.1007/BF00768847.

Lipton, P., 1999. Ischemic cell death in brain neurons. Physiol. Rev. 79 (4), 1431–1568. https://doi.org/10.1152/physrev.1999.79.4.1431.

Mahon, S., Charpier, S., 2012. Bidirectional plasticity of intrinsic excitability controls sensory inputs efficiency in layer 5 barrel cortex neurons in vivo. J. Neurosci. 32 (33), 11377–11389. https://doi.org/10.1523/JNEUROSCI.0415-12.2012.

Mahon, S., Deniau, J.-M., Charpier, S., 2001. Relationship between EEG potentials and intracellular activity of striatal and cortico-striatal neurons: an in vivo study under different anesthetics. Cereb. Cortex 11 (4), 360–373. https://doi.org/10.1093/cercor/11.4.360.

Martin, R.L., Lloyd, H.G.E., Cowan, A.I., 1994. The early events of oxygen and glucose deprivation: setting the scene for neuronal death? Trends Neurosci. 17 (6), 251–257. https://doi.org/10.1016/0166-2236(94)90008-6.

Narayanan, R.T., Udvary, D., Oberlaender, M., 2017. Cell type-specific structural organization of the six layers in rat barrel cortex. Front. Neuroanat. 11 (October), 1–10. https://doi.org/10.3389/fnana.2017.00091.

Nedergaard, M., Hansen, A.J., 1993. Characterization of cortical depolarizations evoked in focal cerebral ischemia. J. Cereb. Blood Flow Metab. 13 (4), 568–574. https://doi.org/10.1038/jcbfm.1993.74.

Oberlaender, M., de Kock, C.P., Bruno, R.M., Ramirez, A., Meyer, H.S., Dercksen, V.J., Helmstaedter, M., Sakmann, B., 2012. Cell type-specific three-dimensional structure of thalamocortical circuits in a column of rat vibrissal cortex. Cereb. Cortex 22 (10), 2375–2391. https://doi.org/10.1093/cercor/bhr317.

O'Connor, D.H., Peron, S.P., Huber, D., Svoboda, K., 2010. Neural activity in barrel cortex underlying vibrissa-based object localization in mice. Neuron. 67 (6), 1048–1061. https://doi.org/10.1016/j.neuron.2010.08.026.

Oostenveld, R., Fries, P., Maris, E., Schoffelen, J.M., 2011. FieldTrip: open source software for advanced analysis of MEG, EEG, and invasive electrophysiological data. Comput. Intell. Neurosci. https://doi.org/10.1155/2011/156869.

Paxinos, G., Watson, C., 2007. The Rat Brain in Stereotaxic Coordinates, 6th edition. Academic Press.

Pietrobon, D., Moskowitz, M.A., 2014. Chaos and commotion in the wake of cortical spreading depression and spreading depolarizations. Nat. Rev. Neurosci. 15 (6), 379–393. https://doi.org/10.1038/nrn3770.

Reig, R., Sanchez-Vives, M.V., Compte, A., Mattia, M., Belmonte, C., 2009. Temperature modulation of slow and fast cortical rhythms. J. Neurophysiol. 103 (3), 1253–1261. https://doi.org/10.1152/jn.00890.2009.

Richter, F., Lehmenkühler, A., 1993. Spreading depression can be restricted to distinct depths of the rat cerebral cortex. Neurosci. Lett. 152 (1–2), 65–68. https://doi.org/10.1016/0304-3940(93)90484-3.

Schramm, A.E., Carton-Leclercq, A., Diallo, S., Navarro, V., Chavez, M., Mahon, S., Charpier, S., 2020. Identifying neuronal correlates of dying and resuscitation in a model of reversible brain anoxia. Prog. Neurobiol. 9–10. https://doi.org/10.1016/j.pneurobio.2019.101733.

Shetty, P.K., Galeffi, F., Turner, D.A., 2012. Cellular links between neuronal activity and energy homeostasis. Front. Pharmacol. 3 MAR (March), 1–14. https://doi.org/10.3389/fphar.2012.00043.

Shlobin, N.A., Aru, J., Vicente, R., Zemmar, A., 2023. What happens in the brain when we die? Deciphering the neurophysiology of the final moments in life. Front. Aging Neurosci. 15 (May), 1–13. https://doi.org/10.3389/fnagi.2023.1143848.

Somjen, G.G., 2001. Mechanisms of spreading depression and hypoxic spreading depression-like depolarization. Physiol. Rev. 81 (3), 1065–1096. https://doi.org/10.1152/physrev.2001.81.3.1065.

Somjen, G.G., 2004. Ions in the Brain: Normal Function, Seizures and Stroke. Oxford University Press.

Steriade, M., 2004. Neocortical cell classes are flexible entities. Nat. Rev. Neurosci. 5 (2), 121–134. https://doi.org/10.1038/nrn1325.

Steriade, M., Timofeev, I., Grenier, F., 2001. Natural waking and sleep states: a view from inside neocortical neurons. J. Neurophysiol. 85 (5), 1969–1985. https://doi.org/10.1152/jn.2001.85.5.1969.

Van Lommel, P., Van Wees, R., Meyers, V., Elfferich, I., 2001. Near-death experience in survivors of cardiac arrest: a prospective study in the Netherlands. Lancet. 358 (9298), 2039–2045. https://doi.org/10.1016/S0140-6736(01)07100-8.

van Rijn, C.M., Krijnen, H., Menting-Hermeling, S., Coenen, A.M.L., 2011. Decapitation in rats: latency to unconsciousness and the "wave of death.". PLoS One 6 (1), 1–6. https://doi.org/10.1371/journal.pone.0016514.

Vicente, R., Rizzuto, M., Sarica, C., Yamamoto, K., Sadr, M., Khajuria, T., Fatehi, M., Moien-Afshari, F., Haw, C.S., Llinas, R.R., Lozano, A.M., Neimat, J.S., Zemmar, A., 2022. Enhanced interplay of neuronal coherence and coupling in the dying human brain. Front. Aging Neurosci. 14 (February), 1–11. https://doi.org/10.3389/fnagi.2022.813531.

Watts, M.E., Pocock, R., Claudianos, C., 2018. Brain energy and oxygen metabolism: emerging role in normal function and disease. Front. Mol. Neurosci. 11 (June), 1–13. https://doi.org/10.3389/fnmol.2018.00216.

Xu, Z.C., Pulsinelli, W.A., 1996. Electrophysiological changes of CA1 pyramidal neurons following transient forebrain ischemia: an in vivo intracellular recording and staining study. J. Neurophysiol. 76 (3), 1689–1697. https://doi.org/10.1152/jn.1996.76.3.1689.

Xu, G., Mihaylova, T., Li, D., Tian, F., Farrehi, P.M., Parent, J.M., Mashour, G.A., Wang, M.M., Borjigin, J., 2023. Surge of neurophysiological coupling and connectivity of gamma oscillations in the dying human brain. Proc. Natl. Acad. Sci. 120 (19) https://doi.org/10.1073/pnas.

Young, J.N., Somjen, G.G., 1992. Suppression of presynaptic calcium currents by hypoxia in hippocampal tissue slices. Brain Res. 573 (1), 70–76. https://doi.org/10.1016/0006-8993(92)90114-O.

Zandt, B.J., ten Haken, B., van Dijk, J.G., van Putten, M.J.A.M., 2011. Neural dynamics during anoxia and the "wave of death.". PLoS One 6 (7), 3–8. https://doi.org/10.1371/journal.pone.0022127.